Lab on a Chip

PAPER

Cite this: *Lab Chip*, 2017, **17**, 2814

An integrated microwell array platform for cell lasing analysis†

Qiushu Chen,[a] Yu-Cheng Chen,[a] Zhizheng Zhang,[b] Biming Wu,[a] Rhima Coleman[a] and Xudong Fan *[a]

Biological cell lasers are emerging as a novel technology in biological studies and biomedical engineering. The heterogeneity of cells, however, can result in various lasing behaviors from cell to cell. Thus, the capability to track individual cells during laser investigation is highly desired. In this work, a microwell array was integrated with high-quality Fabry–Pérot cavities for addressable and automated cell laser studies. Cells were captured in the microwells and the corresponding cell lasing was achieved and analyzed using SYTO9-stained Sf9 cells as a model system. It is found that the presence of the microwells does not affect the lasing performance, but the cell lasers exhibit strong heterogeneity due to different cell sizes, cycle stages and polyploidy. Time series laser measurements were also performed automatically with the integrated microarray, which not only enables the tracking and multiplexed detection of individual cells, but also helps identify "abnormal" cells that deviate from a large normal cell population in their lasing performance. The microarrayed cell laser platform developed here could provide a powerful tool in single cell analysis using lasing emission that complements conventional fluorescence-based cell analysis.

Received 18th May 2017,
Accepted 10th July 2017

DOI: 10.1039/c7lc00539c

rsc.li/loc

Introduction

Cell lasers are emerging as a novel tool in biological studies and biomedical engineering.[1] With intrinsic (fluorescent proteins) or exogenous (dyes) gain medium inside a living cell, laser emission could be generated with merits including threshold-gated emission, narrow linewidth, fingerprint spectral patterns and high sensitivity to dynamic changes of intracellular conditions.[1–5] Thus, cell lasers could have great potential for long-term cell tracking,[2,6] intracellular biomolecular interaction studies and clinical screening.[1]

Currently, there are two major scenarios for cell lasing studies. In the first scenario, microcavities providing optical feedback for laser operation are located inside living cells. By letting cells intake microbeads (5–10 μm in diameter), Humar *et al.* and Schubert *et al.* both observed laser emission from cells.[2,3] Humar *et al.* also demonstrated that oil droplets injected or naturally present in cells could be used for cell lasers.[3] In these works, microbeads and oil droplets serve as ring resonators with high Q whispering-gallery-modes inside cells. This scenario may encounter intrinsic obstacles for biomedical applications. It either relies on cells to intake relatively large ring resonators (diameter >5 μm), which is time-consuming, exhibits low yield and has potential influence on the biological functions of the cells, or applies to only specific types of cells (such as adipocytes). In the second cell lasing scenario, cells containing gain medium are enclosed within an external cavity, which can be a droplet-based ring resonator[7] or a Fabry–Pérot (FP) cavity formed by two highly reflective mirrors.[8] Lasing from cells expressing fluorescent proteins[7,8] or stained with dyes[9,10] was achieved. This scenario is more versatile and can readily be applied to any type of cell. Compared to the droplet-based ring resonator, the FP scheme is easier to implement, and the lasing signal from a specific cell is easier to measure. In earlier cell laser studies with the FP cavity, microbeads slightly larger than a cell (~20 μm in diameter) were mixed with cells to determine the FP cavity length and secure mirror alignment.[8–10] However, in such a bead-defined FP cavity, cells are randomly spread or float on/near the mirror surface, making it difficult to track and monitor cells in a high-throughput and multiplexing manner for an extended duration, which is highly desired in biomedical and biochemical analyses.

While lasing from single cells opens up a new perspective for biochemical analysis, current cell-based lasing technologies are facing difficulties when a large number of cells need to be tested at single cell resolution. No automated and high-throughput detection using the laser approach has been

[a] *Department of Biomedical Engineering, University of Michigan, 1101 Beal Avenue, Ann Arbor, Michigan, 48109, USA. E-mail: xsfan@umich.edu*
[b] *Department of Electrical Engineering and Computer Science, University of Michigan, 1301 Beal Avenue, Ann Arbor, Michigan, 48109, USA*
† Electronic supplementary information (ESI) available. See DOI: 10.1039/c7lc00539c

demonstrated to date. Meanwhile, a microwell array is an attractive platform for cell level studies nowadays, with potential for high-throughput and automated detection. It is capable of capturing and isolating cells and is compatible with imaging and subsequent molecular analysis,[11–14] thus providing information ranging from cell morphology to genomics and proteomes down to the single cell level with high throughput. Microwells are also suitable for long-term monitoring of individual cells for their metabolic activities and response to external stimuli.[15] In this paper, we developed an integrated microwell platform for cell lasing studies using the FP cavity scheme. Microwell arrays were fabricated on top of a highly reflective mirror to capture/locate cells. Lasing from cells in the microwells was achieved and characterized. The microwells provide physical addresses for cells, enabling cell tracking and long-term monitoring during laser interrogation. We further demonstrated that our integrated microwell array cell lasing platform is compatible with automated detection and suitable for high-throughput long-term monitoring, which will bridge the biolaser technology with practical applications.

Experimental

Microwell arrays were fabricated in a biocompatible negative photoresist SU-8 on the surface of dielectric mirrors using standard soft lithography to locate and support cell lasing in this work. 1″ × 1″ dielectric mirrors were obtained from Evaporated Coatings, Inc. (Willow Grove, PA, USA). The mirrors were designed to have a reflection band at 510–550 nm ($R >$ 99.5%) and a transmission band at 460–480 nm ($T >$ 90%). The arrays consisted of microwells with a depth of 25 μm and a diameter of 35 μm. To access wells more easily during experiments, every 10 × 10 wells were grouped into a sub-array in the design. The spacing between wells within a sub-array was 65 μm and the spacing between sub-arrays was 500 μm. The microwell fabrication procedures are described as follows. The mirrors were first cleaned by solvent ultrasonication (sonicated in acetone, ethanol and de-ionized water sequentially) and oxygen plasma treatment. Then, they were dehydrated at 150 °C for 15 minutes right before a 25 μm thick SU-8 2025 (MicroChem Corp., USA) layer was spin-coated on top. After soft-baking the SU-8-coated mirrors for 3 minutes at 65 °C and 8 minutes at 95 °C, a contact lithography tool Karl Suss MA 45S was used to UV expose the mirrors through a mask with the microwell array design. The exposed mirrors were subsequently subjected to post-exposure baking at 65 °C for 1 minute and 95 °C for 6 minutes, followed by 8 minutes of development. After rinsing and drying, the SU-8 microwell array on top of the mirror could be clearly seen under a microscope. The microwell arrays were further hard baked at 150 °C for 10 minutes and treated with oxygen plasma to improve hydrophilicity before loading with cells.

Lasing from cells has successfully been demonstrated with various cell types and gain media over the past few years,[8–10] showing versatility that can be further explored for bio-photonic studies and biochemical analysis. As a model system, in this work, Sf9 insect cells were used and stained with a green DNA dye, SYTO9 (Thermo Fisher Scientific, USA), to demonstrate cell lasing in the microwell array platform. SYTO9 is a widely used live cell staining dye that is membrane-permeable and turns into the fluorescent state when it binds with DNA/RNA. The DNA/RNA-specific nature of SYTO9 makes the laser gain potentially relevant to the physiological status of cells. For staining, Sf9 insect cells were first washed with HBSS buffer and re-suspended to a concentration of 1×10^6 cells per ml. Then, SYTO9 was added to a final concentration of 25 μM. After 10 minutes of incubation, cells were washed with HBSS to get rid of the excess dye and re-suspended in the culture medium for their best viability. Fig. 1(a) shows the steps of loading the cells into the microwells and subsequent laser excitation/detection. Stained cells were added to the microwell array pre-wetted with the culture medium at a surface density of 400 cells per mm^2 and set still for 5 minutes for them to reach the bottom of the wells. Then, the cells not captured by a microwell were removed using a cell culture scraper. Finally, a plane mirror was placed on top of the loaded array, thus forming an FP cavity with the substrate mirror. The mirror–microwell–mirror structure was held by a pair of 3D-printed holders for better mechanical stability and reduced buffer evaporation during the experiment. Note that the Sf9 cells are suspension cells under the current conditions. Without the confinement of the microwells, these cells could move around in the presence of flow or mechanical disturbance.

For laser experiments, a typical confocal setup (Fig. 1(b)) was used to excite cells in the wells and collect the emission signal. An optical parametric oscillator (OPO) pulsed laser at 475 nm (5 ns pulse width and 20 Hz repetition rate) was used as the excitation source. The excitation spot size was 60 μm in diameter, slightly larger than the well diameter in order to illuminate the entire well homogeneously. The laser emission from cells was collected using a Horiba iHR 550 spectrometer with the entrance slit set to 0.3 mm in order to collect the signal from the entire 35 μm well area of interest. The mirror holder was mounted on a motorized 2D translation stage to precisely position the well of interest under the excitation beam.

Results

Lasing from both suspension and adherent cells in an FP cavity was demonstrated previously, with a typical lasing threshold around 100 μJ mm^{-2}.[8–10] However, cells were randomly located on/near the mirror surface in those studies. In this work, SU-8 microwell arrays were used to locate the cells and track the cell lasing performance in an automated and high-throughput manner. We first demonstrated and characterized the lasing emission from the captured cells in the microwells. The SU-8 microwell arrays defined the distance between the substrate and the top mirror, hence the cavity length. Under the present loading conditions (400 cells per

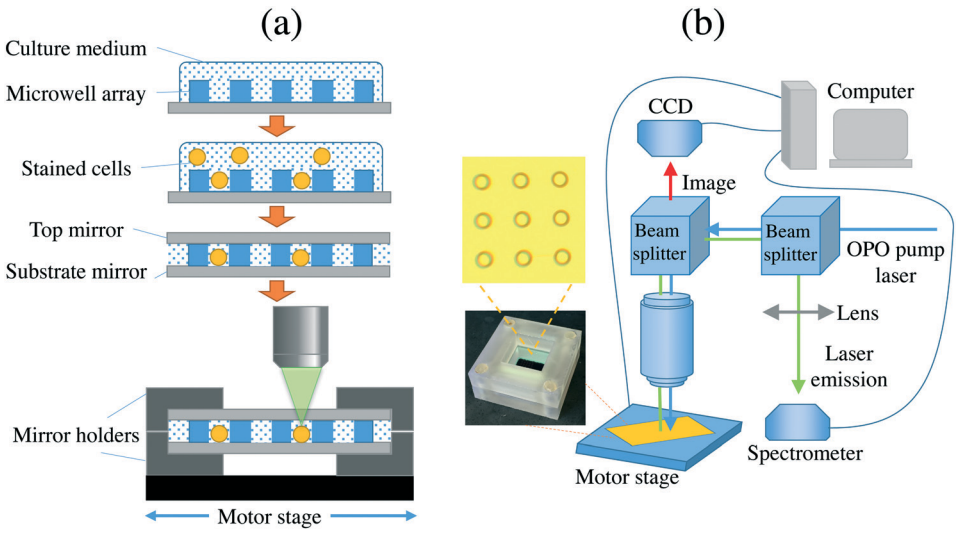

Fig. 1 (a) Steps for loading cells into the microwell array. (b) Detection system for cell lasing in the microwell array. Inset: photo of the microwell-based FP cavity held in the mirror holder and the microscope view of the microwells.

mm^2) and considering that there are 100 wells (a 10 × 10 array) in an area of 1 mm^2, we expected that about 40 cells can be captured in 100 wells (total area of 100 wells × 400 cells per mm^2 ~40) and 30 out of them can be captured as singlets according to the Poisson distribution. Our experimental observation that approximately 30% of the wells were occupied by single cells agreed with the above calculation. Lasing from SYTO9-stained cells in the well was achieved, as shown in Fig. 2, with a lasing wavelength ranging from 530 nm to 550 nm and a threshold around 60 μJ mm^{-2}. The lasing wavelength was red shifted about 30 nm from the fluorescence maximum of SYTO9, which is typical for dye lasing. The relatively low threshold compared to those of previously reported cell lasers resulted mainly from the high abundance of DNA stained with SYTO9 in the nuclei. The effective dye concentration was estimated to be on the order of mM given the genome size of Sf9 (~1.6 × 10^9 bp)[16] and the association constant of SYTO9 (1.8 × 10^5 M^{-1}).[17] The free spectral range (FSR) of the lasing modes was around 3.5 nm, corresponding to a cavity length of 30 μm (assuming that the effective refractive index of the cavity is 1.36 in the presence of a cell). The slightly increased cavity length compared to the SU-8 thickness might result from a thin culture medium layer between the SU-8 and the top mirror.

About 30% of cells captured in the microwells could lase under 130 μJ mm^{-2} excitation. Fig. 3(a) plots the histogram of the lasing threshold for the lasing cells in the microwells, showing the lasing threshold that could range from 20 μJ mm^{-2} to 100 μJ mm^{-2}. This heterogeneity in the lasing threshold is attributable to different DNA concentrations inside nuclei that depend highly on the size of the nuclei, the cell cycle stages and the polyploidy that is generally observed in Sf9 cells due to their chromosome instability.[18] For comparison, the SYTO9-stained cells were also tested in a bead-based FP cavity similar to that in ref. 8 (bead size 30 μm in diameter in the current work) and a similar percentage of cells (26%) were found to lase under 130 μJ mm^{-2} excitation. The histogram of the lasing threshold for the lasing cells is plotted in Fig. 3(b) and shows virtually no difference from the microwell case, suggesting that the microwell structures

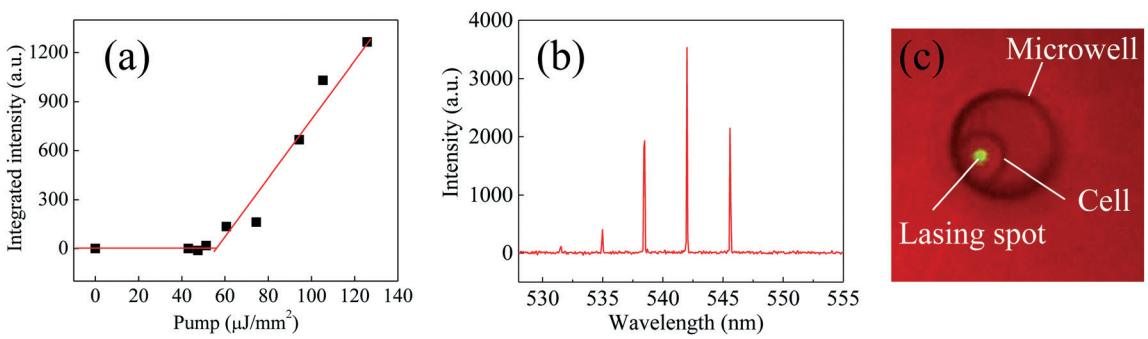

Fig. 2 Lasing threshold (a) and lasing spectrum (b) of a cell captured in the microwell. (c) CCD image of the lasing cell. The red color results from mirrors rejecting green color in the illumination light coming from the bottom. Fluorescence from the cell is also filtered out by the mirror and therefore only a strong lasing signal is detected and shown in the image.

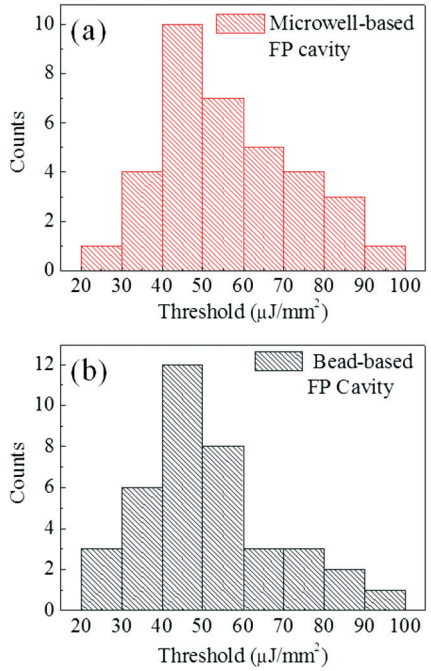

Fig. 3 Histograms of the lasing thresholds for (a) the cells captured in a microwell array and (b) the cells, along with beads, randomly spread on top of the mirror.

do not have any impact on cell lasing behavior. This is expected since the lasing modes of cells are mainly confined by the mirrors and the cells themselves. The confinement of the microwell structure on the lasing modes is negligible, given the relatively large size of the wells compared to the cells and the low reflectivity on the boundary between SU-8 and water. We also conducted a diffraction simulation of a Gaussian excitation beam normal to the mirror, showing that the presence of the microwell structure does not affect the excitation conditions of the cell laser (ESI,† Fig. S1).

It is known that the cell has a slightly larger refractive index than the surrounding culture medium, which provides the lensing effect for stabilizing the FP cavity and makes lasing insensitive to mirror misalignment (tilt tolerance ~0.5 degrees).[10] Consequently, the *Q*-factor for each microwell is determined mainly by the reflectivity of the mirrors and the optical characteristics of the cell itself (such as gain, absorption and scattering). In our experiment, the empty cavity *Q*-factor in the absence of a cell is estimated to be over 6×10^4 according to the cavity length of 30 μm and the round-trip loss of <1%. With a cell present, the *Q*-factor drops to 1×10^4 due to the ~5% round-trip loss from the cell.[10] Therefore, the cell lasing performance (*e.g.*, the lasing threshold or efficiency) can be used to reveal the gain and loss present in a cell, which can vary significantly with cellular conditions such as the morphology, cell cycle, metabolic status and polyploidy. Such variations have already manifested themselves in the lasing threshold distribution in Fig. 3, highlighting the strong need for the ability to track individual cells and perform highly multiplexed detection on a large cell population.

After lasing measurement, the top mirror was replaced by a transparent cover glass and the conventional fluorescence image of the cells in the well was taken. Thanks to the microwells, the cells residing in the microwells were not disturbed, thus allowing us to compare side-by-side the fluorescence image with the laser image, as illustrated in Fig. 4, which verifies that the laser indeed occurred in the heavily stained nucleus region. Further comparison shows that there are specific patterns that could be identified in the laser image. For example, in Fig. 4(a) and (b), the cells mainly support (1,1) Ince–Gaussian modes.[8,19,20] In Fig. 4(c), the (0,0) mode is supported instead. However, in the fluorescence images, all three cells show only one stained nucleus without any details. The difference in laser images could result from a combined effect of the cell morphology and the refractive index[21] and the gain distribution inside a cell, which can vary significantly throughout the cell cycle. Thus, the laser-based detection, with the aid of microwell arrays, may provide a new approach for better understanding of cells.

The pre-defined positions of microwells in an array also make it possible to perform high-throughput, automatic laser detection. To implement this, a LabView program was used to coordinate the 2D motorized translation stage, the spectrometer and the imaging CCD. The position accuracy of the translation stage was characterized, showing a center-to-center difference of <5 μm between different wells. With a fixed pump intensity of 130 μJ mm^{-2}, a 10 × 10 well array loaded with SYTO9-stained Sf9 cells was screened and the emission spectrum and the CCD image of each well were collected automatically. It took 5 minutes to screen the whole array in the current setup, which can be further shortened with a more advanced automation system. Fig. 5 shows the screening results. The numbers in the table (Fig. 5(a)) represent the peak values in each spectrum. To determine whether a cell is lasing, the cut-off value is set at three standard deviations of the background noise (50 in this example). The highlighted regions in the table indicate that there were cells lasing at corresponding microwells. The FSR of the lasing mode was measured to be 3.51 nm across the entire array, which confirms the identical optical conditions for all microwells. Together with the CCD image of each microwell, we can study the lasing population and the status of lasing cells statistically. In this example, there were 28 wells occupied by single cells, 10 of which could lase, while 13 wells were occupied by double cells and 8 of the total 26 cells could lase. The overall lasing ratio was 33%, which agreed well with the manually measured results. There was no significant difference in the lasing ratio between the one-cell-in-a-well and two-cells-in-a-well cases, indicating that the lasing behavior of a cell was independent of its neighbor cell.

We further demonstrated that the automatic scanning microwell array enables high-throughput time-series monitoring of cell lasing behavior. One cell-loaded array was continuously scanned over 25 minutes and the lasing characteristics (such as the spectrum and image) of each cell were tracked. The pump intensity was fixed at 130 μJ mm^{-2}. There were 55

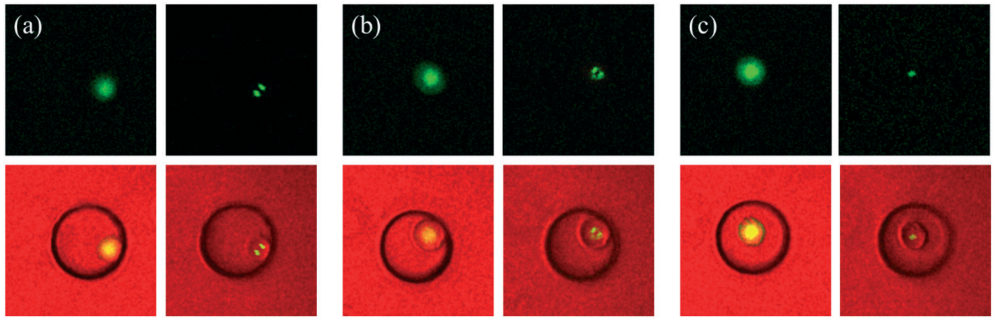

Fig. 4 (Top row) Fluorescence (left) and lasing (right) images of three different cells (a–c) captured in three different microwells. (Bottom row) Corresponding bright-field images, where fluorescence (left) and laser emission (right) are superimposed for better visualization and comparison.

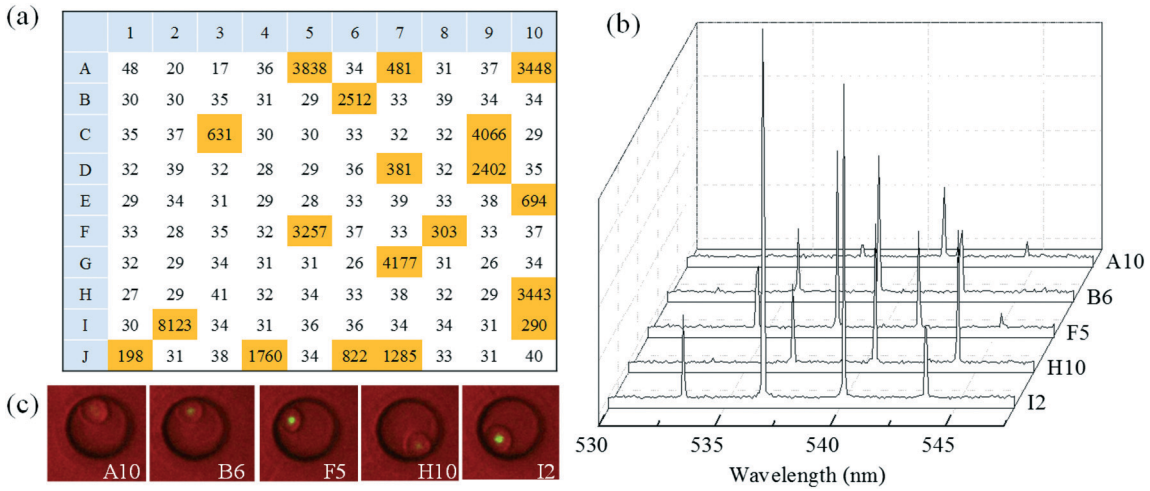

	1	2	3	4	5	6	7	8	9	10
A	48	20	17	36	3838	34	481	31	37	3448
B	30	30	35	31	29	2512	33	39	34	34
C	35	37	631	30	30	33	32	32	4066	29
D	32	39	32	28	29	36	381	32	2402	35
E	29	34	31	29	28	33	39	33	38	694
F	33	28	35	32	3257	37	33	303	33	37
G	32	29	34	31	31	26	4177	31	26	34
H	27	29	41	32	34	33	38	32	29	3443
I	30	8123	34	31	36	36	34	34	31	290
J	198	31	38	1760	34	822	1285	33	31	40

Fig. 5 Results of automatic scanning. (a) Heat map of the lasing array. Data shows the spectral peak value of each well. The yellow-highlighted boxes denote the microwells that exhibit cell lasing. (b) Sample spectra of lasing wells identified by their row/column number given in the *y* axis. (c) Corresponding lasing images with illumination light on. OPO excitation = 130 μJ mm^{-2}. CCD exposure time = 100 ms.

cells captured in the wells in this case (41 singlets, 7 doublets), 17 of which could lase at the beginning. Cells with a relatively low lasing intensity ceased to lase gradually during monitoring due to photobleaching of SYTO9. There were 9 cells with identifiable lasing peaks throughout the entire monitoring process, 7 out of which were found to have unchanged lasing patterns in both the spectrum and the CCD image. A representative sample (cell in well E5) is shown in Fig. 6(a) and (b). According to Fig. 6(a), while the FSR of the cell laser remains virtually the same throughout the entire 25 minutes of the experiment, there is a gradual blue-shift of the lasing wavelength between 0 min and 20 min and a reverse trend (red-shift) from 20 min to 25 min. Although the detailed mechanisms for the blue- and red-shifts are still unclear to us, they occur consistently for all 7 cells under study, as shown in Fig. 6(c). We speculate that this systematic drift in our experimental conditions might be caused by buffer evaporation and a concomitant salt concentration increase, which change the cavity length and the buffer's refractive index. Ambient temperature fluctuation might also contribute to the lasing wavelength shift (see discussion in the ESI†). However, we found little contribution of photobleaching to the wavelength shift, because no shift was observed in the photostability test (ESI,† Fig. S2) and in fact dyes contributed only to a very small amount of the materials that fill the cavity in this study. Note that the relatively large variance in the wavelength shift is observed for the 15–20 min and the 20–25 min groups, which is caused by the cells in microwells B5, I7 and J10. Since B5 and I7/J10 were tested at the beginning and at the end of each scan, our relatively slow scanning speed (5 minutes) might not be able to catch up with the systematic change in experimental conditions discussed above.

Based on the work in Fig. 6, a reference baseline can be established and help identify and analyze cells that have "deviated" or "abnormal" lasing behavior. Fig. 7 shows evolving lasing characteristics of the 2 "abnormal" cells from the same microwell array as in Fig. 6. For cell B6 in Fig. 7(a), the lasing mode shown in the lasing images changes from the Ince–Gaussian (2,2) mode to higher order modes and eventually to the (0,0) mode. For cell F4 in Fig. 7(b), the initial Ince–Gaussian (1,1) mode rotates 90° and is replaced by the Ince–Gaussian

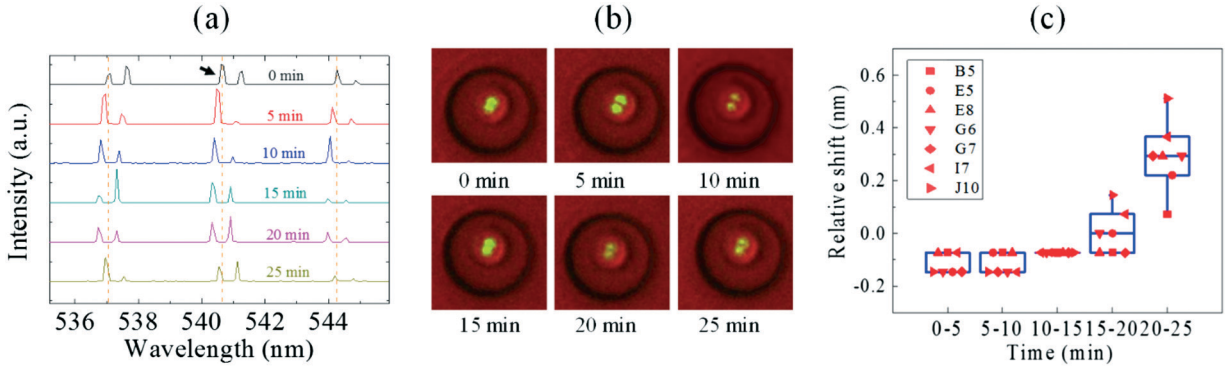

Fig. 6 (a) Lasing spectra of a cell captured in a microwell (E5) in long-term monitoring. OPO excitation = 130 μJ mm^{-2}. Curves are vertically shifted for clarity. The arrow indicates the peak whose wavelength was tracked. (b) Corresponding images of the cell, showing that the lasing pattern remained unchanged during the entire 25 minutes of experiment. The green channel is enhanced for better visualization of the lasing modes. (c) Boxplot of the wavelength increment of every 5 minute interval for a lasing peak near 540 nm for 7 cells (in microwells B5, E5, E8, G6, G7, I7 and J10, respectively) on the same array. A positive/negative increment denotes a red/blue shift in wavelength.

(0,0) mode. Fig. 7 plots the relative position (with respect to that at 0 min) of a lasing peak marked by arrows in (a) and (b) for both cells. A reference curve derived from Fig. 6(c) is also plotted as a benchmark to indicate the collective response of the "normal" cells to the systematic changes. It is obvious that these two "abnormal" cells have different and opposite responses. The lasing modes in the B6 cell are more resistant to the systematic changes, and the lasing peaks barely shift before the pattern changes. In contrast, the lasing modes in the F4 cell turn out to be more susceptible and shift a relatively large amount before we lose track of the modes. Humar *et al.* reported the change in cell lasing patterns by changing the buffer's refractive index outside the cell.[10] However, in our case, the changes in the effective refractive index (caused by the thermo-optical effect and buffer salt concentration) and the cavity length were identical across the entire array and were verified to be negligible (<0.1%) according to Fig. 6, and thus cannot explain the deviations in the lasing behavior of these two cells. Possible reasons could be the dynamic change of cellular geometry, the integrity of the nucleus (the nucleus may be broken down following apoptosis[22]) and photobleaching of dyes that consequently changes the gain profile within the cell. To fully understand the lasing pattern shift, detailed quantification of the cell sizes, the DNA concentration/distribution and the difference in responsiveness of cells to external stimuli (heat, osmotic pressure change, *etc.*) is essential. On the other hand, the existence of such "abnormal" lasing cells shows the need for and the potential of using the lasing cell array to study the inhomogeneity within a cell population.

The cell, together with its subcellular structures such as the nucleus, is a naturally formed complex optical system. By specifically staining the components inside a cell, a spatially varying gain profile can be achieved in a cell laser system. For example, when the nucleus is specifically stained as in this work, the gain is limited to a region smaller than the cavity formed by the entire cell and the two parallel mirrors. Such a configuration has been shown to favor the operation of high-order Laguerre–Gaussian modes in a stable cavity[23] and has also been utilized in the generation of Ince–Gaussian modes.[24] Similarity can be drawn between the SYTO9-stained Sf9 cells and the lasing system with a tightly confined gain

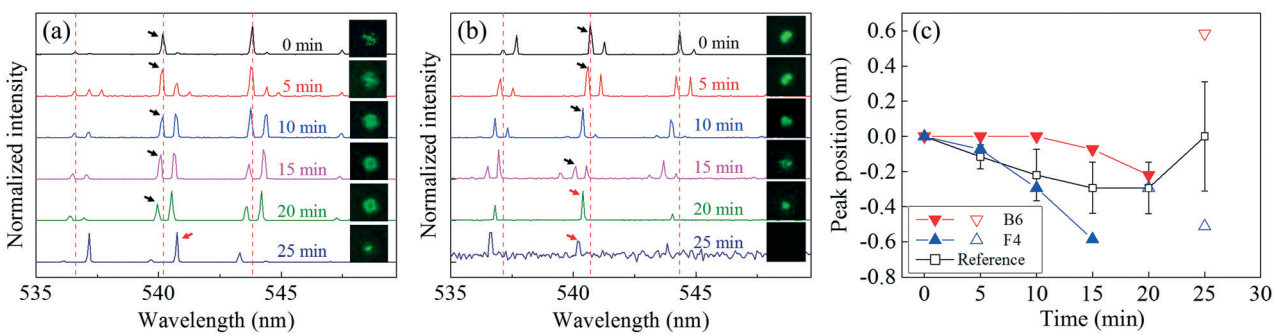

Fig. 7 Spectra of the cell from microwell B6 (a) and microwell F4 (b) showing evolving lasing patterns during long-term monitoring. Arrows mark the peaks that were tracked. Inset: The corresponding lasing patterns extracted from CCD images and enhanced for better visualization. (c) Relative positions of the marked peaks in (a) and (b) during monitoring. The black curve corresponds to the reference baseline derived from the 7 cells shown in Fig. 6(c). Error bars show the 95% confidence interval. Hollow symbols correspond to peaks marked by red arrows in (a) and (b), which are likely different modes from those marked by black arrows.

profile reported in ref. 24 since the Ince–Gaussian modes are commonly observed in our work (see Fig. 6 and 7). Therefore, it is possible to use the laser mode to extract the gain distribution and reconstruct cellular structures/geometries, such as the size and the nuclear–cytoplasmic ratio of the cell.

Conclusions

In summary, we have prototyped and characterized an automated, integrated microwell array platform for systematic and statistical studies of cell lasers. The microwell array does not affect the cell lasing performance, but makes the captured cells more resistant to disturbance, thus allowing us to track individual cells and performing various analyses on them. It further enables the establishment of a reference baseline that represents the collective responses of cells to a change in an overall environment and the identification of rare "abnormal" cells that deviate from a large cell population. The microwell array is readily compatible with other technologies such as hyperspectral imaging,[8] polarization analysis and temporal profile studies.[4] Further integration of microfluidic channels that facilitate cell incubation, drug treatment[25] and downstream processing and analysis[11,14] will open the door to applying the cell lasing approach to single cell analysis and drug screening.

Acknowledgements

This work was supported by the National Science Foundation (ECCS-1607250). The Lurie Nanofabrication Facility of the University of Michigan is greatly appreciated for microwell array fabrication.

References

1 X. Fan and S. H. Yun, *Nat. Methods*, 2014, **11**, 141–147.
2 M. Schubert, A. Steude, P. Liehm, N. M. Kronenberg, M. Karl, E. C. Campbell, S. J. Powis and M. C. Gather, *Nano Lett.*, 2015, **15**, 5647–5652.
3 M. Humar and S. Hyun Yun, *Nat. Photonics*, 2015, **9**, 572–576.
4 J. A. Rivera and J. G. Eden, *Opt. Express*, 2016, **24**, 10858–10868.
5 M. Aas, Q. Chen, A. Jonas, A. Kiraz and X. Fan, *IEEE J. Sel. Top. Quantum Electron.*, 2016, **22**, 1–15.
6 M. Schubert, K. Volckaert, M. Karl, A. Morton, P. Liehm, G. B. Miles, S. J. Powis and M. C. Gather, *Sci. Rep.*, 2017, **7**, 40877.
7 A. Jonas, M. Aas, Y. Karadag, S. Manioglu, S. Anand, D. McGloin, H. Bayraktar and A. Kiraz, *Lab Chip*, 2014, **14**, 3093–3100.
8 M. C. Gather and S. H. Yun, *Nat. Photonics*, 2011, **5**, 406–410.
9 S. Nizamoglu, K.-B. Lee, M. C. Gather, K. S. Kim, M. Jeon, S. Kim, M. Humar and S.-H. Yun, *Adv. Opt. Mater.*, 2015, **3**, 1197–1200.
10 M. Humar, M. C. Gather and S.-H. Yun, *Opt. Express*, 2015, **23**, 27865–27879.
11 J. Yuan and P. A. Sims, *Sci. Rep.*, 2016, **6**, 33883.
12 S. M. Schubert, S. R. Walter, M. Manesse and D. R. Walt, *Anal. Chem.*, 2016, **88**, 2952–2957.
13 A. Morimoto, T. Mogami, M. Watanabe, K. Iijima, Y. Akiyama, K. Katayama, T. Futami, N. Yamamoto, T. Sawada, F. Koizumi and Y. Koh, *PLoS One*, 2015, **10**, e0130418.
14 A. J. Hughes, D. P. Spelke, Z. Xu, C.-C. Kang, D. V. Schaffer and A. E. Herr, *Nat. Methods*, 2014, **11**, 749–755.
15 P. Zhang, J. Zhang, S. Bian, Z. Chen, Y. Hu, R. Hu, J. Li, Y. Cheng, X. Zhang, Y. Zhou, X. Chen and P. Liu, *Lab Chip*, 2016, **16**, 2996–3006.
16 V. Bernal, N. Carinhas, A. Y. Yokomizo, M. J. T. Carrondo and P. M. Alves, *Biotechnol. Bioeng.*, 2009, **104**, 162–180.
17 S. M. Stocks, *Cytometry, Part A*, 2004, **61**, 189–195.
18 R. F. Jarman-Smith, S. J. Armstrong, C. J. Mannix and M. Al-Rubeai, *Biotechnol. Prog.*, 2002, **18**, 623–628.
19 M. Karl, C. P. Dietrich, M. Schubert, I. D. W. Samuel, G. A. Turnbull and M. C. Gather, *J. Phys. D: Appl. Phys.*, 2017, **50**, 084005.
20 M. A. Bandres and J. C. Gutiérrez-Vega, *Opt. Lett.*, 2004, **29**, 144–146.
21 P. Y. Liu, L. K. Chin, W. Ser, H. F. Chen, C. M. Hsieh, C. H. Lee, K. B. Sung, T. C. Ayi, P. H. Yap, B. Liedberg, K. Wang, T. Bourouina and Y. Leprince-Wang, *Lab Chip*, 2016, **16**, 634–644.
22 S. Elmore, *Toxicol. Pathol.*, 2007, **35**, 495–516.
23 C. J. Flood, G. Giuliani and H. M. van Driel, *Opt. Lett.*, 1990, **15**, 215–217.
24 U. T. Schwarz, M. A. Bandres and J. C. Gutiérrez-Vega, *Opt. Lett.*, 2004, **29**, 1870–1872.
25 Z. Zhang, Y.-C. Chen, Y.-H. Cheng, Y. Luan and E. Yoon, *Lab Chip*, 2016, **16**, 2504–2512.

